




Classical and semiclassical calculations of state-selective cross sections for electron capture and excitation in $\text{Be}^{4+} + \text{H}(2s)$ collisions

A. Jorge, Clara Illescas , and L. Méndez 

*Laboratorio Asociado al CIEMAT de Física Atómica y Molecular en Plasmas de Fusión
and Departamento de Química, Módulo 13, Universidad Autónoma de Madrid, Cantoblanco, E-28049 Madrid, Spain*

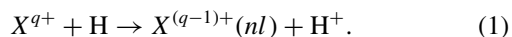
 (Received 20 October 2021; accepted 15 December 2021; published 18 January 2022)

A computational study of $\text{Be}^{4+} + \text{H}(2s)$ collisions has been carried out. Two computational models have been employed: the classical trajectory Monte Carlo (CTMC) method and the numerical solution of the time-dependent Schrödinger equation (GTDSE). The integral n and nl partial cross sections for H excitation and electron capture, obtained with both methods, are compared at two energies: 20 and 100 keV/u. It is shown that the CTMC, with an improved hydrogenic initial distribution, provides excitation cross sections in good agreement with the numerical calculation for excitation to $\text{H}(n)$ with $n > 3$. The agreement between the corresponding nl partial cross sections from both methods is less satisfactory at 100 keV/u, where there is a transition from the low-energy mechanism that involves an increase of the populations with l , and the high-energy mechanism, where the dipole-allowed transitions are dominant. The electron capture cross sections calculated with the CTMC method do not depend on the initial distribution and show a reasonable agreement with the GTDSE ones, which supports the use of the CTMC method to calculate electron capture cross sections into highly excited levels and total cross sections. The mechanism of the electron capture process is discussed and CTMC calculations of the ionization process are also presented.

DOI: [10.1103/PhysRevA.105.012811](https://doi.org/10.1103/PhysRevA.105.012811)

I. INTRODUCTION

Collisions between multiply charged ions and hydrogen atoms are relevant in tokamak plasmas. In particular, the measurement of impurity densities is usually carried out by applying the charge-exchange recombination spectroscopy (CXRS) technique [1], where a fast beam of H atoms is injected in the plasma. The atoms collide with the plasma ions, X^{q+} , giving rise to the electron capture (EC) processes:



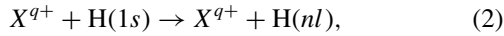
The EC yields $X^{(q-1)+}$ in excited states, the emission of which is employed to determine ion densities [2]. The method requires accurate cross sections for the EC processes. In this respect, a recent work [3] has pointed out significant differences in Ar densities obtained from two sets of EC cross sections. On the other hand, the collisions between beam atoms and plasma particles can excite the H atoms. It is well known that the cross sections for EC from $\text{H}(2s)$ are large and a small fraction of excited H can significantly modify the effective emission coefficients employed in CXRS [4,5]. The accurate determination of EC cross sections for collisions with excited H is therefore required. The application of the CXRS diagnostics also requires the knowledge of beam densities that can be obtained by means of the beam emission spectroscopy. The application of this technique is based on collisional-radiative models, the accuracy of which also relies on that of the underlying atomic data [6], including cross sections for excitation and ionization in H collisions with plasma ions. Collisions with Be ions are particularly relevant

because Be is a plasma facing material of tokamaks, which has motivated new calculations of state-selective cross sections [7–9]. In this respect, collisions of Be^{4+} ions with H are the benchmark systems of the Coordinated Research Project of the IAEA Data for Atomic Processes of Neutral Beams in Fusion Plasma.

In this paper we discuss the accuracy of two methods to calculate collision cross sections: the classical trajectory Monte Carlo (CTMC) and a semiclassical method based on the numerical solution of the time-dependent Schrödinger equation (GTDSE). The CTMC [10] has been applied in several works to calculate EC total and partial cross sections. In the CTMC the electron wave function is replaced by a classical distribution made up of an ensemble of electron trajectories. The original method (m-CTMC) employs an initial microcanonical distribution formed by trajectories with the energy of the initial quantal level. The microcanonical momentum distribution is exact, but the tail of the quantal radial distribution is not correctly described. Alternative initial distributions have been proposed that improve the radial distributions without significantly modifying the momentum distribution [11–13]. In this respect, we have constructed the hydrogenic distributions of this paper as explained in Ref. [14]. The CTMC method with a hydrogenic initial distribution (h-CTMC) has been successfully applied to calculate ionization, and total and state-selective EC cross sections for collisions of several multicharged ions with $\text{H}(1s)$ [14–18]. In general, the CTMC is a fast method, particularly useful to calculate partial EC cross sections to populate very excited states. The application of the CTMC method to collisions with $\text{H}(n = 2)$ has been

considered in Refs. [18,19]; these works pointed out that the differences between h-CTMC and m-CTMC cross sections for EC and ionization are smaller than those found for collisions with H(1s). Recently, Ziaean and Tórkésy [7] have reported EC cross sections for $\text{Be}^{4+} + \text{H}(2l)$ calculated using the m-CTMC method.

Excitation cross sections in collisions of multiply charged ions with H(1s) have been studied in several works. Janev and Presnyakov [20] proposed a scaling law based on the application of the dipole approximation, the validity of which was discussed in Refs. [21–23]. Suarez *et al.* [24] calculated the cross sections for the excitation cross sections



with $n \leq 6$, for collisions with $X^{q+} = \text{Li}^{3+}$, Ne^{10+} , Ar^{18+} , using both h- and m-CTMC. They compared the results with those from a one-center expansion in terms of spherical Bessel functions, previously used in Ref. [25]. They found that the m-CTMC systematically underestimates the excitation cross sections. The h-CTMC showed better agreement with the one-center expansion. In the present paper we consider the application of these two CTMC treatments to Be^{4+} collisions with H(2s).

The GTDSE method involves the numerical solution of the eikonal equation, which is formally identical to the time-dependent Schrödinger equation. Numerical methods have been previously applied to ion-atom collisions in several works [26–28]. In these calculations, the initial collision wave function is evaluated in the points of a three-dimensional (3D) lattice, which is then propagated in time. We have applied the GTDSE method to collisions of Be^{4+} with H(1s) [29], where we checked the accuracy of other treatments and estimated the uncertainties of the EC cross sections. The recent calculation of Antonio *et al.* [9] using a different semiclassical model has reported EC cross sections in good agreement with those of Ref. [29]. In the present paper we have extended the method to evaluate excitation cross sections. In practice, the calculation involves the use of two reference frames, one with the H fixed on the origin, to calculate excitation cross sections, and another one, with the Be nucleus on the origin, to calculate EC cross sections, as previously applied for ion-molecule collisions [30]. In general, the systematic application of the GTDSE to obtain cross sections is not feasible since it requires large memory allocation and lengthy time propagations, particularly for collisions involving excited states. Therefore, our aim is to apply the method for some energies to check the accuracy of the CTMC and other calculations.

Besides excitation and EC, we have calculated ionization cross sections. In this case, we have carried out only CTMC calculations, which in previous calculations have been shown to correctly describe the ionization mechanism at the collision energies of the present paper.

The paper is organized as follows: In Sec. II we summarize the GTDSE and CTMC methods. In Sec. III we present n - and nl partial cross sections for excitation, and in Sec. IV we present the partial cross sections for electron capture. In Sec. V we discuss our results for total cross sections for excitation, electron capture, and ionization. A summary of the paper is presented in Sec. VI. Atomic units are employed unless otherwise stated.

II. METHODS

A. The GTDSE method

At the energies considered in this paper one can employ the semiclassical impact parameter approximation, where the nuclei follow rectilinear trajectories defined by $\mathbf{R}(t) = \mathbf{b} + \mathbf{v}t$, with \mathbf{b} the impact parameter and \mathbf{v} the relative velocity. The electronic motion is then described by the wave-function $\Psi(\mathbf{r}, t)$ solution of the semiclassical equation

$$\left[H_{\text{el}} - i \frac{\partial}{\partial t} \right] \Psi = 0 \quad (3)$$

with the electronic Hamiltonian

$$H_{\text{el}}[\mathbf{r}, \mathbf{R}(t)] = -\frac{1}{2} \nabla_{\mathbf{r}}^2 + V_{\text{H}} + V_{\text{Be}} + \frac{4}{R} \quad (4)$$

where \mathbf{r} is the electron position vector, and V_{H} and V_{Be} are the potentials for the electron interaction with both nuclei.

In the treatment of $\text{Be}^{4+} + \text{H}(2s)$ collisions, the H nucleus is initially on the origin of the laboratory reference frame with $\hat{Z} \parallel \hat{v}$ and $\hat{X} \parallel \hat{b}$, and \hat{Y} is perpendicular to the collision plane. The origin of the electronic coordinates is also in the H nucleus. At large internuclear separations, the wave function is a linear combination of the atomic orbitals ϕ_{2s} and ϕ_{2p} , with $\tilde{\phi}_{2p}$ a p orbital in the direction of the internuclear vector \mathbf{R} :

$$\tilde{\phi}_{2p} = \frac{b}{R} \phi_{2px} + \frac{vt}{R} \phi_{2pz}. \quad (5)$$

The perturbation responsible for the Stark mixing of the $n = 2$ orbitals is

$$H_S = -\frac{Q\mathbf{r} \cdot \hat{\mathbf{R}}}{R^2}, \quad (6)$$

where $Q = 4$ is the projectile charge. The integration of (3) in the $\{\phi_{2s}, \tilde{\phi}_{2p}\}$ basis with $\lim_{t \rightarrow -\infty} \Psi(\mathbf{r}, t) = \phi_{2s} e^{-iE_2 t}$ leads to

$$\Psi_s(\mathbf{r}, t) = (\cos \xi \phi_{2s} + i \sin \xi \tilde{\phi}_{2p}) e^{-iE_2 t}, \quad (7)$$

where

$$\xi(t) = \frac{Q\mu}{bv} \left[\tan^{-1} \left(\frac{vt}{b} \right) + \frac{\pi}{2} \right]. \quad (8)$$

E_2 is the energy of the level H($n = 2$), and

$$\mu = \langle \phi_{2s} | \mathbf{r} \cdot \hat{\mathbf{R}} | \tilde{\phi}_{2p} \rangle = 3a_0. \quad (9)$$

The numerical integration starts at a distant point of the trajectory, $Z_0 = vt_0$, where the electron transfer is negligible, the two-state approximation is valid, and therefore the wave function is $\Psi_s(\mathbf{r}, t_0)$.

In the present paper, we have employed the parallel GRIDTSE package [31], modified in Refs. [29,32], to solve numerically Eq. (3). The wave function Ψ is evaluated at the points of a 3D Cartesian lattice. The lattice representation of the electronic wave function is a vector Ψ solution of the matrix equation

$$\mathbf{H}\Psi = (\mathbf{T} + \mathbf{V})\Psi = i\dot{\Psi}. \quad (10)$$

\mathbf{V} is a diagonal matrix that stores the values of the potential $V_{\text{Be}} + V_{\text{H}}$ at the grid points, while the kinetic-energy matrix, \mathbf{T} , is a nondiagonal sparse matrix that is obtained by applying the finite differences method (see Ref. [33]), considering

TABLE I. Soft-core parameters ϵ_H and ϵ_{Be} [Eq. (11)] employed for different grid densities.

Δ_q (a.u.)	ϵ_H	ϵ_{Be}
0.2 (G1)	3.66×10^{-3}	5.19×10^{-3}
0.4 (G2)	1.12×10^{-3}	8.89×10^{-3}

a stencil of $n_s = 15$ neighboring grid points. Equation (10) is time integrated by applying the second-order differences method with time steps of the order of 10^{-2} a.u., during which the electron-nuclei Coulomb attraction terms are approximately constant.

The extension of the grid is taken as $-L_{\max} \leq q \leq L_{\max}$, $q = x, z$ and $0 \leq y \leq L_{\max}$, where we have taken advantage of the symmetry of the Hamiltonian upon reflection in the collision plane (XZ). The present calculations were carried out with a broad box of $L_{\max} = 80 a_0$. Such an extension allows the description of the Be^{3+} orbitals up to the quantum level $n \leq 11$. As a final remark, according to the uncertainty principle, the time step employed in the time integration is directly related to the grid spacing [34]. Therefore, as the description of the wave function in the spatial coordinates improves with increasing density, shorter time steps must be employed.

In practice, as in previous numerical treatments [28], a soft-core approximation is introduced to allow the integration near the Coulomb singularity. The potentials are

$$V_H(\mathbf{r}, \mathbf{R}(t)) = -\frac{1}{(r^2 + \epsilon_H)^{1/2}},$$

$$V_{Be}(\mathbf{r}) = -\frac{4}{(|\mathbf{r} - \mathbf{R}|^2 + \epsilon_{Be})^{1/2}}, \quad (11)$$

and the soft-core parameters $\epsilon_{H,Be} \ll \Delta_q$ have been optimized by fitting the atomic energies for each grid density (Table I), with deviations smaller than 1% from the exact energies. In order to avoid unphysical reflections at the walls of the box, we have introduced the mask function [32,35]:

$$M(\mathbf{r}) = \prod_{i=1,3} \begin{cases} \exp\{-\alpha(|q_i| - L_{\max} + \delta)^2\} & \text{if } L_{\max} - |q_i| < \delta \\ 1 & \text{elsewhere} \end{cases}$$

with $\delta = 3.0 a_0$ and $\alpha = 0.002 a_0^{-2}$. As pointed out in previous works [36,37], mask functions used in grid schemes are directly related to complex absorbing potentials.

The original reference system, with the origin on the proton, allows us to evaluate excitation probabilities. In the limit $t \rightarrow \infty$, part of the initial electron density has been removed by electron capture and ionization, and in the numerical treatment is absorbed by the mask function. The probability of finding the H atom in a given state Φ_{nlm}^H is

$$P_{nlm}^H = \lim_{t \rightarrow \infty} |\langle \Phi_{nlm}^H | \Psi \rangle|^2. \quad (12)$$

As in previous applications [30], we calculate the electron capture cross sections by moving the origin of the electron coordinate system to the Be nucleus. In our calculations, the origin is changed at $Z_1 = vt_1 = -30 a_0$, when the EC process has not started yet. After changing the origin, we carry out the

numerical integration with the initial condition:

$$\Psi(\mathbf{r}, t_1) = \Psi_H(\mathbf{R}_1 - \mathbf{r}_{Be}) \exp(i\mathbf{v} \cdot \mathbf{r}_{Be} - \frac{1}{2}v^2 t_1) \quad (13)$$

that includes a plane-wave translation factor. Here the function Ψ_H has been obtained by propagating $\Psi_s(\mathbf{r}, t_0)$ from t_0 to t_1 with the origin on the H nucleus, and $\mathbf{R}_1 = \mathbf{b} + \mathbf{v}t_1$. During the numerical calculation that starts at $t = t_1$, the Be^{4+} nucleus remains fixed at the origin and the H^+ follows the straight-line trajectory. The electron density, initially attached to the H^+ nucleus, is partially transferred to Be^{4+} . In the limit $t \rightarrow \infty$, the H^+ has left the box, and the electron density inside it corresponds to electron capture. The remaining electron density, which is absorbed by the mask functions, includes the density that is joined to the H^+ after the collision, the ionizing density, and the capture into excited states of Be^{3+} , which cannot be described by the finite extension of the lattice. The EC probabilities are

$$P_{nlm}^{Be} = \lim_{t \rightarrow \infty} |\langle \Phi_{nlm}^{Be} | \Psi \rangle|^2 \quad (14)$$

where Φ_{nlm}^{Be} are the Be^{3+} wave functions.

The integral cross sections for excitation and capture are then obtained as

$$\sigma_{nlm} = 2\pi \int_0^\infty b P_{nlm} db, \quad (15)$$

where P_{nlm} are the excitation [Eq. (12)] or EC [Eq. (14)] probabilities. The probabilities, P_{nl} , and cross sections, σ_{nl} , for transition into the subshell nl are

$$P_{nl} = \sum_{m=-l}^{+l} P_{nlm}, \quad \sigma_{nl} = \sum_{m=-l}^{+l} \sigma_{nlm} \quad (16)$$

and analogously, for the transition to shell n ,

$$P_n = \sum_{l=0}^{n-1} P_{nl}, \quad \sigma_n = \sum_{l=0}^{n-1} \sigma_{nl}. \quad (17)$$

To follow the time evolution of the collision wave function it is useful to introduce the projections $\langle \phi_{nlm}^H | \Psi \rangle$ for excitation, and $|\langle \phi_{nlm}^{Be} | \Psi \rangle|$ for EC. The functions

$$\zeta_{nl}^{H,Be}(t) = \sum_{m=-l}^{+l} |\langle \phi_{nlm}^{H,Be} | \Psi \rangle|^2 \quad (18)$$

for projection on a given subshell will be employed in Secs. III and IV to discuss the mechanisms of these processes.

B. The CTMC method

The eikonal CTMC method has been explained in previous works. Essentially, we assume rectilinear nuclear trajectories as in the GTDSE method, and we describe the electronic motion by a classical distribution $\rho(\mathbf{r}, \mathbf{p}, t)$. Initially, ρ is a microcanonical distribution function, $\rho^m(\mathbf{r}, \mathbf{p})$, in which all the electron trajectories have the energy, ϵ , of the initial state of the target atom. The distribution has been discretized in terms of $N = 2 \times 10^6$ noninteracting trajectories and the Hamilton equations have been integrated from $t_{ini} = -500/v$ a.u. up to $t_{fin} = \frac{1000}{v}$ a.u. We have checked the convergence of the total and partial cross sections with respect to the statistics

and the integration time. In particular, the long collision time ensures that the calculation correctly takes into account the Stark mixing.

We have also employed a hydrogenic initial distribution. The hydrogenic distribution [11] is constructed as a linear combination with constant coefficients of microcanonical distributions with different energies, ϵ_k :

$$\rho^h(\mathbf{r}, \mathbf{p}) = \sum_k a_k \rho_k^m(\mathbf{r}, \mathbf{p}). \quad (19)$$

The coefficients of the combination are obtained [11,14,38] by imposing that the average energy is equal to that of the corresponding quantum level, ϵ . It is also ensured that the distributions included in the combination fulfill the conditions [39,40]

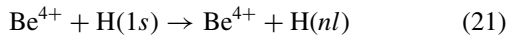
$$\begin{aligned} [(n-1/2)(n-1)n]^{1/3} < n_k \leq [(n+1/2)(n+1)n]^{1/3}, \\ \frac{l}{n} < \frac{l_c}{n_k} \leq \frac{l+1}{n}, \end{aligned} \quad (20)$$

where, in atomic units, $n_k^2 = -\frac{Z^2}{2\epsilon_k}$ and l_c is the classical value of the electronic angular momentum. These conditions permit us to divide the phase space into adjacent nonoverlapping bins associated to the quantum numbers n and l . In practice, the use of the hydrogenic distribution improves the results with respect to those of the microcanonical calculation for electron capture and ionization processes, and n partial electron capture cross sections for relatively large n in ion-H(2s) collisions (see Refs. [29,41]). Previous calculations [18,19] show that the improvement is less important for collisions with H($n=2,3$) than for collisions with H in the ground state. In the present paper, we have carried out the calculations for collisions with H(2s) by including in the initial distribution only the trajectories with l_c fulfilling (20) with $l=0$.

III. EXCITATION CROSS SECTIONS

A. Excitation in $\text{Be}^{4+} + \text{H}(1s)$ collisions

We have considered the reactions



by applying the GTDSE method. Since the extension of the initial $1s$ orbital is smaller than that of the $2s$ orbital, we have employed a box of $L_{\max} = 40 a_0$ ($80 a_0$ for collisions with $2s$), but a higher density $\Delta_q = 0.2 a_0$ is required to accurately represent the initial wave function. This grid was previously employed for the calculation of electron capture cross sections in Ref. [29]. The cross sections are compared with previous calculations in Fig. 1. Good agreement is found with previous close-coupling calculations, and the agreement is less satisfactory with the calculation of Rodríguez and Miraglia [42] at low energies, as expected for a perturbative calculation. We find a remarkable agreement with the nl -resolved cross sections obtained in the one-center expansion of Errea *et al.* [25], which supports the application of the GTDSE method for calculating excitation cross sections. We do not include in this illustration the CTMC results since, as explained in Ref. [24], the m-CTMC underestimates the excitation because of the already mentioned difficulty of the microcanonical distribution that does not reproduce the tail of the quantal radial

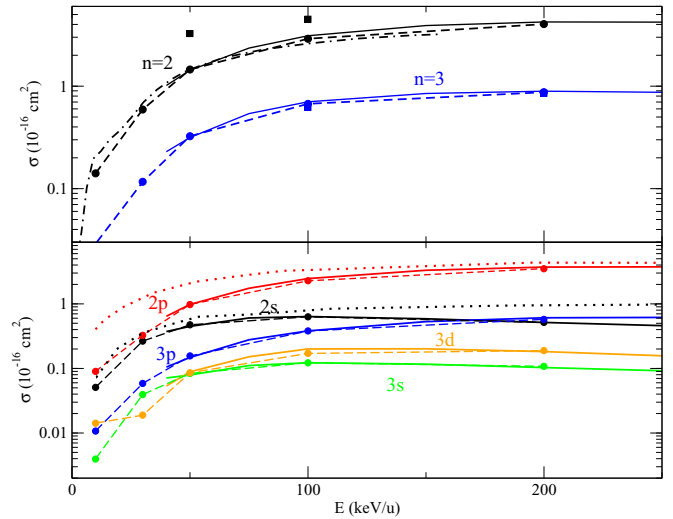
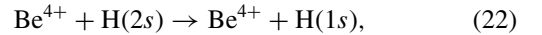


FIG. 1. Total cross sections for H excitation in collisions of Be^{4+} with H(1s). (—●—), GTDSE calculations; ■, eikonal impulse approximation [42] (---), one-center close-coupling calculation [25]; (-·-·-), molecular orbital calculation [44]; (···), QTMC-KW calculation [43].

distribution. In contrast, the h-CTMC overestimates the cross section because of the large contributions of trajectories near the upper limit of the $1s$ bin in (20). The recent results of Ref. [43] for excitation into $2s$ and $2p$ overestimate those from the semiclassical calculations.

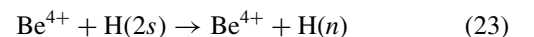
The nl partial cross sections of Fig. 1 show that in general the dipole-allowed transition to $l=1$ is dominant. It can be noted that the cross section for excitation into H(2s) is identical to that for the inverse process:



but the result plotted in Fig. 1 is more accurate than that obtained in the calculation of Sec. III B, starting from the $2s$ orbital, because the higher grid density of the calculation provides a better description of the $1s$ orbital.

B. Excitation in $\text{Be}^{4+} + \text{H}(2s)$ collisions

The cross sections σ_n for the excitation reactions



are displayed in Fig. 2 for two collision energies. The CTMC method allows us to consider excitations to very high n , while the length of the box ($L_{\max} = 80 a_0$) precludes accurate computation of the cross sections for excitation into $n > 5$ with the GTDSE method. However, some conclusions can be drawn from the comparisons. The GTDSE and h-CTMC agree for $n=4,5$, which supports the accuracy of both results. As already explained for the excitation $n=1 \rightarrow n=2$, the h-CTMC calculation overestimates the cross section for the excitation reactions $n=2 \rightarrow n=3$ because the electron trajectories near the limit of the classical $n=2$ bin lead to an artificial increase of the excitation. Nevertheless, the m-CTMC cross section $2s \rightarrow n=3$ does not exhibit this unphysical behavior, but the incorrect description of the tail of the radial distribution yields a general underestimate of the

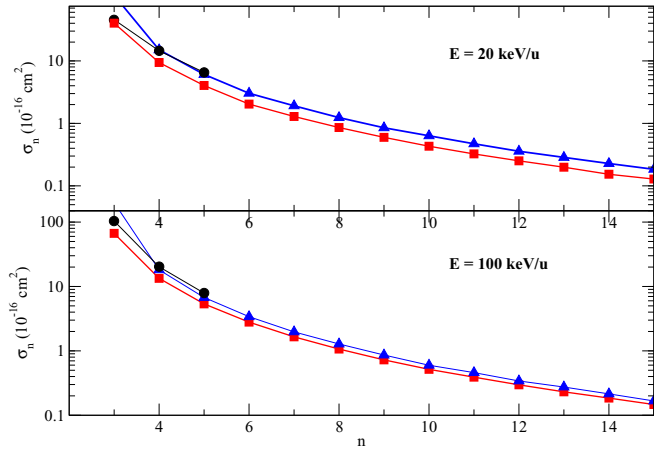


FIG. 2. Total cross sections for excitation in collisions of Be^{4+} with $\text{H}(2s)$. (—●—), GTDSE calculations; ■, m-CTMC; ▲, h-CTMC.

excitation cross sections, similar to that found in previous calculations [23,24]. In conclusion, the GTDSE is useful to check the accuracy of the CTMC calculations and is the only calculation that provides an accurate value of the $n = 2 \rightarrow n = 3$ cross section. For excitation into $n \geq 4$ the h-CTMC method is appropriate.

We show in Figs. 3 and 4 the nl resolved excitation cross sections, σ_{nl} , for the two energies of Fig. 2. Although the h-CTMC calculation overestimates the cross section for excitation into $n = 3$, the l distribution is similar to that found in the other calculations and we have included the h-CTMC cross sections in these figures. At $E = 20$ keV/u, we find a general good agreement between GTDSE and h-CTMC values of σ_{4l} and σ_{5l} while the m-CTMC underestimates these cross sections. The cross sections σ_{3l} of Fig. 3 show that the dipole-forbidden transition to $3d$ is dominant, as previously found in the calculation of Ref. [42]. Analogously, our calculations of σ_{nl} for $n \geq 4$ lead to l distributions with maxima at $l = 3$ or 4. Also, the nl partial cross sections for $n > 6$, calculated only with the CTMC method and not shown in the

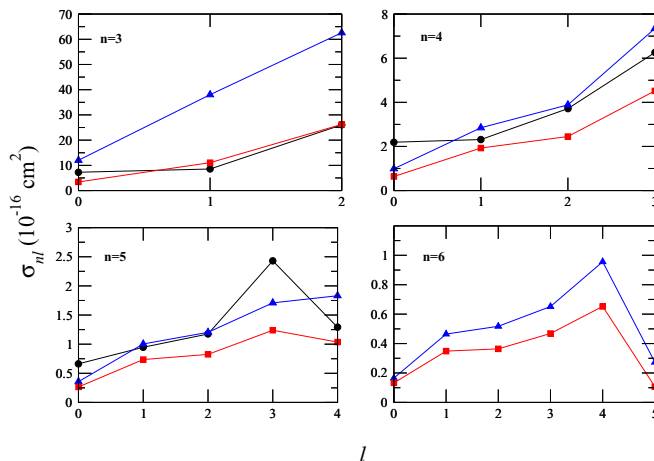


FIG. 3. Total cross sections for excitation to $\text{H}(nl)$ in collisions of Be^{4+} with $\text{H}(2s)$ at $E = 20$ keV/u. ●, GTDSE; ■, m-CTMC; ▲, h-CTMC.

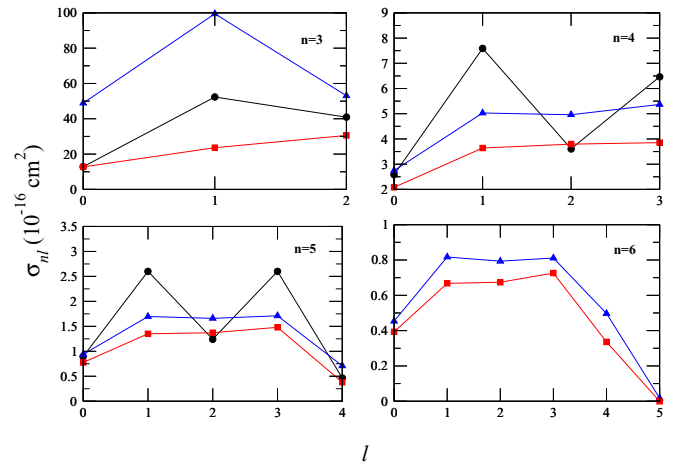


FIG. 4. Total cross sections for H excitation to $\text{H}(nl)$ in collisions of Be^{4+} with $\text{H}(2s)$ at $E = 100$ keV/u. Symbols as in Fig. 3.

figure, have maxima at $l = 4$. It can be noted that the results of Ref. [45] for $\text{H}^+ + \text{H}$ collisions also indicated the breakdown of the dipole selection rule.

The comparison of Figs. 3 and 4 points to a shift of the l distributions to lower values of l as E increases. In particular, the maximum of the σ_{3l} is found at $l = 1$ for $E = 100$ keV/u. We observe in Fig. 4 that the CTMC calculations yield σ_{nl} for $n \geq 4$ with a plateau for $1 \leq l \leq 3$, while the GTDSE results exhibit two local maxima at $l = 1$ and 3. At both energies the cross sections σ_{n0} are relatively small, which is an expected result since these subshells have only one state. With respect to the comparison of the results with the three methods, the nl partial cross sections at $E = 100$ keV/u do not show a clear indication of the accuracy of the three calculations, but we think that the agreement of GTDSE and h-CTMC n partial cross sections for $n = 4, 5$, together with the known limitation of the m-CTMC method, suggest that the h-CTMC is more accurate to calculate the cross sections for excitation into nl subshells with $n > 3$.

The semiclassical calculation provides the transition probabilities and the projections of the collision wave functions on the atomic orbitals, as functions of $Z = vt$ (the *history* of the collision). In this respect, to better understand the populations of the subshells $4l$ with $l = 1, 2$, and 3, we have plotted these two parameters in Figs. 5 and 6. In Fig. 5, we show the opacity functions $bP_{4l}(b)$ [Eq. (12)] at the two energies of the present calculation. We highlight, on the one hand, how the higher cross section for $l = 1$ at 100 keV/u comes mainly from the higher probability at large impact parameters. On the other hand, we highlight how the probabilities of populating the $l = 2$ and 3 states are similar at the two impact energies, but shifted to the left (making the $l = 1$ subshell the most probable for high b) at 100 keV/u. To understand how the different states are populated during the collision, we plot in Fig. 6 the functions $\zeta_{nl}^{\text{H}}(t)$ of (18). We display in Fig. 6 the populations of the initial $2s - 2p$ states, as well as those of $l = 1, 2$ (and 3) for $n = 3$ and 4 and $b = 24 a_0$. The $l = 0$ populations have not been included for the sake of clarity. First, we want to draw attention to the crossing point between $\zeta_{20}^{\text{H}}(t)$ and $\zeta_{21}^{\text{H}}(t)$ for 20 keV/u. As it can be seen, this

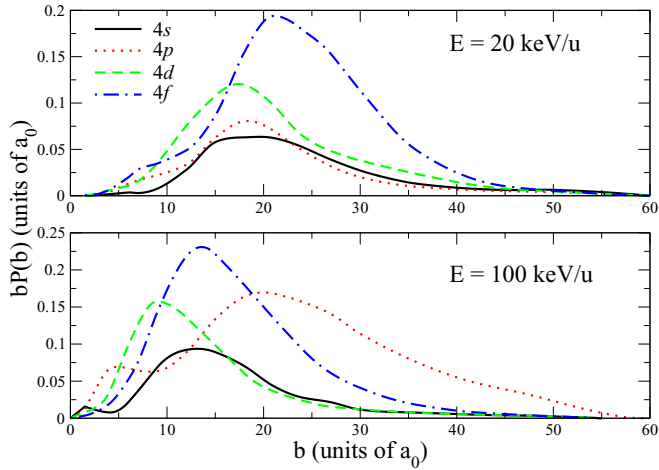


FIG. 5. Opacities $bP_{4l}(b)$ [Eq. (16)] as functions of the impact parameter b for impact energies 20 and 100 keV/u.—, 4s; ···, 4p; — — —, 4d; ····, 4f.

crossing point does not occur at 100 keV/u for this impact parameter. For all the shells considered, the $l = 1$ populations are dominant for those impact parameters where there is no crossing point between $\zeta_{20}^H(t)$ and $\zeta_{21}^H(t)$. At $E = 20$ keV/u this does not happen at any b , while for 100 keV/u we find this crossing point for $b \lesssim 20 a_0$. Before the crossing point, the np populations are also the largest ones for each n , indicating that the $2s \rightarrow np$ are the most important ones. When the crossing point appears, the excitation takes place mainly from the $2p$ orbitals, and the main excitation transition is $2p \rightarrow 3d$. One can notice in Fig. 6 that the $4f$ state is more rapidly populated than the $4d$. The $3d$ subshell is at the same time populating the $4f$ and taking most of the $l = 2$ contribution coming from $2p$.

Another significant fact is that for 20 keV/u the statistical behavior (increasing probability for increasing l 's) is still im-

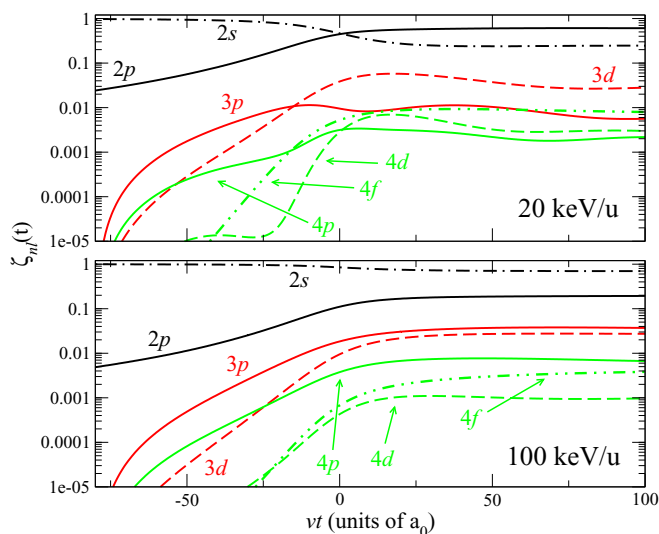


FIG. 6. The populations ζ_{nl}^H [Eq. (18)] as functions of vt for impact energies of 20 and 100 keV/u and $b = 24 a_0$. Black lines, $n = 2$; red lines, $n = 3$; blue lines, $n = 4$.—, p states; — — —, d states; ····, f states; ···, $2s$.

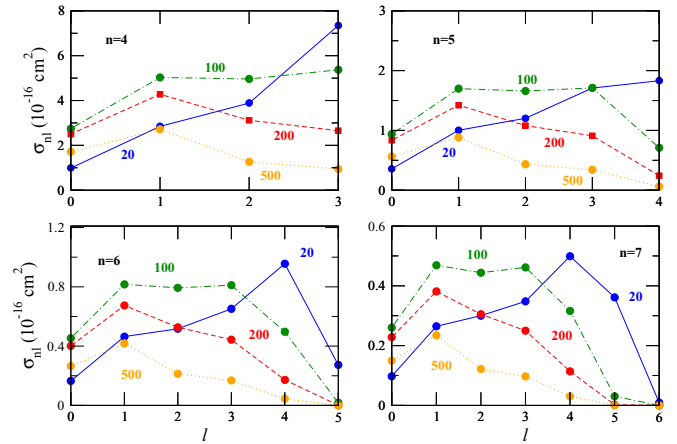


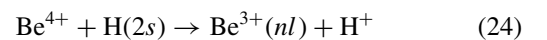
FIG. 7. Total cross sections for excitation to $H(nl)$ ($n = 4-7$) in collisions of Be^{4+} with $\text{H}(2s)$, calculated with the h-CTMC method for four collision energies (20, 100, 200, and 500 keV/u), as indicated in the figure.

portant while this effect is less significant for 100 keV/u, and we can start seeing the perturbative behavior which should be dominant for higher impact velocities. When the perturbative regime starts being dominant we can expect the $l = 1$ state to be the most populated, as well as the disappearance of the differences between $l = 2$ and 3. The two peaks in the nl -excitation cross sections for 100 keV/u (Fig. 4) can be seen as the result of the dying of the statistical regime while the perturbative regime struggles to be born.

We find a similar behavior of the h-CTMC partial cross sections at 100 keV/u. Although the two maxima for $l = 1$ and 3 can be slightly distinguishable in $\sigma_{5,6l}$ (Fig. 4), they are clear for $n > 7$, not shown in the figure. To further illustrate the transition between the more statistical distribution to the perturbative behavior, we show in Fig. 7 the h-CTMC values for σ_{nl} at four impact energies: 20, 100, 200, and 500 keV/u. In this figure not only are the two maxima for $l = 1$ and 3 more clearly shown for 100 keV/u, but also the expected maximum at $l = 1$ (and decreasing σ_{nl} for higher l 's) appears for 200 keV/u, and is definitely clear at 500 keV/u, as expected. The extension of the h-CTMC calculation to higher energies thus confirms the proposed mechanism.

IV. ELECTRON CAPTURE PARTIAL CROSS SECTIONS

We have calculated the cross sections for the electron capture reactions



using the GTDSE method and the CTMC with both micro-canonical and hydrogenic initial distributions. The comparison between the n partial cross sections is shown in Fig. 8. The GTDSE calculation supports the classical calculation for $n \leq 11$, with a somewhat better agreement with the h-CTMC. The box size used in the GTDSE calculation precludes the calculation for $n \leq 11$, but the agreement with the CTMC calculation allows us to use the latter to provide cross sections at high n . It can be noted that the maximum cross section

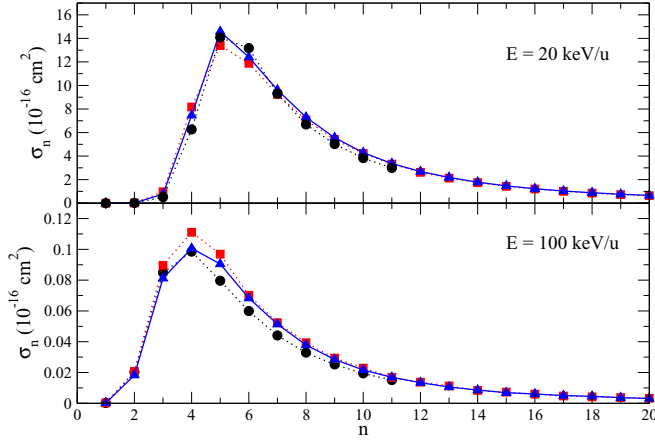


FIG. 8. n partial total cross sections for electron capture in collisions of Be^{4+} with $\text{H}(2s)$ at $E = 20$ and 100 keV/u. (—●—), GTDSE calculations; ■, m-CTMC calculation; ▲, h-CTMC calculation.

appears at the same n_{max} for the three calculations ($n_{\text{max}} = 5$ for $E = 20$ keV/u, $n_{\text{max}} = 4$ for $E = 100$ keV/u).

The partial nl cross sections are displayed in Figs. 9 ($E = 20$ keV/u) and 10 ($E = 100$ keV/u). The agreement between the two methods is remarkable, although slight shifts of the maxima of the l distributions are noticeable. At $E = 20$ keV/u we find the maxima of the cross sections at $l_{\text{max}} = 5$ for $n > 7$ and $l_{\text{max}} = n - 1$ for $n < 7$ in both methods. At $E = 100$ keV/u, we obtain $l_{\text{max}} = 4$ in the CTMC calculation and $l_{\text{max}} = 3$ in the GTDSE one for $n \geq 6$. These partial cross sections are qualitatively similar to that found in Ref. [18] for collisions of C^{6+} and N^{7+} with $\text{H}(n = 2)$, and l_{max} approaches the value $q^{3/4}$ suggested in Ref. [39], at $E = 100$ keV/u. We have also checked that the nl partial cross sections of Ref. [7] are practically identical to those of our m-CTMC calculation for $n = 2-4$.

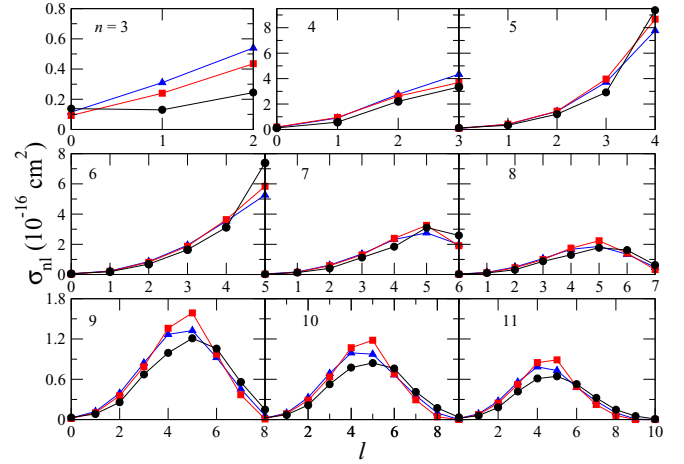


FIG. 9. nl partial total cross sections for electron capture in collisions of Be^{4+} with $\text{H}(2s)$ at $E = 20$ keV/u. (—●—), GTDSE calculations; ■, m-CTMC calculation; ▲, h-CTMC calculation.

To further discuss the mechanism of the EC process, we have considered, as for the excitation reactions, the corresponding histories of the collision obtained in the GTDSE calculation. As in our previous discussion of the excitation reaction, we have studied the time evolutions of $\zeta_{nl}^{\text{Be}}(t)$ of Eq. (18). At $E = 100$ keV/u (Fig. 11), we find that the capture starts in the neighborhood of the point of closest approach $t = 0$. For each b , the EC probability on a given n is mainly determined by the values of $\zeta_{nl}^{\text{Be}}(t = 0)$ with a redistribution between the different nl subshells in the collision way out, where the transitions take place with $\Delta l = \pm 1$. The time evolution clearly shows that the maxima of $\zeta_{nl}^{\text{Be}}(t = 0)$ are in general obtained for the value of l which leads to a maximum of the radial components R_{nl} of the orbitals ϕ_{nlm} at $r_{\text{Be}} = b$. To further analyze this point, we consider the functions ζ_{nl}^{Be} of Eq. (18); they can be expressed as

$$\zeta_{nl}^{\text{Be}} = \sum_{m=-l}^{+l} |\langle \phi_{nlm}^{\text{Be}} | \Psi \rangle|^2 = \left\langle \Psi \left[\sum_{m=-l}^{+l} |\phi_{nlm}^{\text{Be}} \rangle \langle \phi_{nlm}^{\text{Be}}| \right] \Psi \right\rangle = \langle \Psi | \mathcal{P}_{nl} | \Psi \rangle. \quad (25)$$

Writing the orbitals as products of radial functions and spherical harmonics, we obtain

$$\mathcal{P}_{nl}\Psi = \int dr r^2 R_{nl}(r') R_{nl}(r) \sum_{m=-l}^{+l} \int d\Omega Y_{lm}(\Omega') Y_{lm}(\Omega) \Psi(r, \Omega), \quad (26)$$

where we have simplified the notation by writing $\mathbf{r} \equiv \mathbf{r}_{\text{Be}}$. Using the addition theorem for the spherical harmonics,

$$\mathcal{P}_{nl}\Psi = \frac{(2l+1)}{4\pi} \int dr r^2 R_{nl}(r') R_{nl}(r) \int_0^{2\pi} d\phi \int_0^\pi d\theta \sin\theta P_l(\cos\gamma) \Psi(r, \theta, \phi), \quad (27)$$

where

$$\cos\gamma = \cos\theta \cos\theta' + \sin\theta \sin\theta' \cos(\phi - \phi'), \quad (28)$$

and P_l is a Legendre polynomial.

Near the point of closest approach, the function Ψ is not very different from the initial $2s$ orbital, and the maximum value of Ψ is found in the H nucleus. Therefore, the maximum projection is obtained for the value of l that has a maximum

of R_{nl} in the H nucleus. We have found some exceptions to this general rule at relatively large impact parameters, where the largest maximum of R_{nl} corresponds to low l 's, and the statistical weight $2l + 1$ is important; for instance, for $b = 7$ and $n = 4$, the values of $R_{4l}(r = b)$ for $l = 0-2$ are larger than that of $R_{43}(r = b)$ while $\zeta_{43}(t \approx 0)$ is larger than the other ζ_{4l} .

The collision *histories* at $E = 20$ keV/u show that the EC process starts at $t < 0$ as expected for a more adiabatic

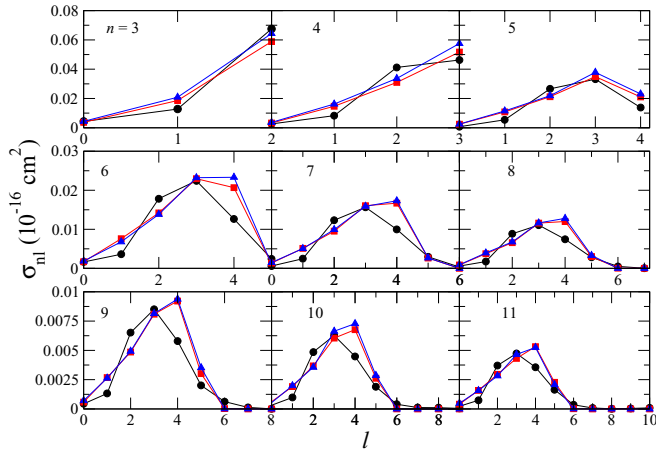


FIG. 10. nl partial total cross sections for electron capture in collisions of Be^{4+} with $\text{H}(2s)$ at $E = 100$ keV/u. (—●—), GTDSE calculations; ■, m-CTMC calculation; ▲, h-CTMC calculation.

transition that involves the polarization and delocalization of the initial wave function, but the distributions between the nl subshells follow a behavior similar to that described at high energies.

V. TOTAL CROSS SECTIONS

We plot in Fig. 12(a) our h-CTMC total EC cross sections. The m-CTMC cross sections are indistinguishable from the h-CTMC, and the very small differences are illustrated at $E = 20$ and 100 keV/u in panels (b) and (c). The good agreement between the EC results with both distributions for ion collisions with $\text{H}(n = 2)$ has been previously pointed out in Refs. [18,19], and is consistent with the small differences between the partial cross sections of Sec. IV. Our total CTMC cross sections also show very good agreement with the recent CTMC calculation of Ref. [7]. However, we find noticeable differences with the Atomic Orbital Close Coupling calculation of Igenbergs [46], which may be due to an overpopulation of the excited levels of Be^{3+} in that calculation, as previously found in Ref. [29]. To further analyze the accuracy of the classical and semiclassical calculations, we have plotted in Fig. 12 our GTDSE results. The limited extension of the box precludes calculation of the EC cross sections into $\text{Be}^{3+}(n > 11)$; however, the good agreement with the CTMC partial cross sections allows us to estimate the total cross section by adding the GTDSE cross section for EC into $\text{Be}^{3+}(n \leq 11)$ and the h-CTMC cross sections into $\text{Be}^{3+}(n > 11)$. The estimates shown in Figs. 12(b) and 12(c) indicate that, at these energies, the differences between both calculations are smaller than 13% and these differences can be traced back to those for the n values near the maxima of the n distributions of Fig. 8. We have checked that the uncertainties due to the final integration time ($Z = 100 a_0$) of the n partial cross sections are smaller than 1% in the GTDSE calculation.

The accurate calculation of total cross sections for excitation is difficult with all the available methods. The semiclassical calculations, either the close-coupling calculations [24] or the numerical methods, provide the partial cross sections for excitation into low n shells, but not for populating

high n levels. In contrast, the h-CTMC overestimates the cross section for excitation into $\text{H}(n = 3)$, leading to an inaccurate total cross section. In order to estimate the total cross section for $\text{H}(2s)$ excitation, we have combined the results of both calculations. Taking into account that GTDSE and h-CTMC show good agreement for $n = 4, 5$ (Fig. 2), we have estimated the total cross section by adding the GTDSE partial cross sections for $n = 3, 4, 5$ and the h-CTMC ones for $n > 6$. The results for $E = 20$ and 100 keV/u of Fig. 12(a) show the importance of the excitation process that becomes dominant at $E = 100$ keV/u.

The GTDSE method does not provide an accurate total cross section for ionization because the electronic flux that leaves the box (in practice is removed by the mask function) includes ionization but also excitation into high n levels and electron capture, and these contributions cannot be separated. In contrast, the CTMC method easily provides these cross sections. Moreover, as already found in previous works [18,19], the known difficulties of the initial microcanonical distribution are not relevant for collisions with excited targets, and m-CTMC and h-CTMC agree. The two CTMC results are almost indistinguishable in Fig. 12, with differences between both calculations of about 5%. The cross sections tabulated in Ref. [46] are very small. This underestimate is similar to that found for $\text{C}^{6+} + \text{H}$ collisions in Ref. [18].

VI. SUMMARY AND CONCLUSIONS

We have carried out a computational study of $\text{Be}^{4+} + \text{H}(2s)$ collisions by employing a semiclassical method (GTDSE), where the eikonal equation is solved numerically in a 3D grid, and the CTMC method. In the application of the GTDSE method we have started the numerical integration at a distant point $Z_0 = -80 a_0$, where a perturbative two-state approximation is valid and the collision wave function is given by the Stark mixing of $2s$ and $2p$ orbitals. We have carried out two separate GTDSE calculations. In the first one, the origin of electron coordinates is placed on the H nucleus, and allows us to calculate excitation cross sections; in the second one, the origin is placed on Be^{4+} , and yields electron capture cross sections.

The CTMC method is comparatively very fast and we have started the integration of the electron trajectories at very large distances, and checked the convergence with respect to the initial integration time. The CTMC calculations start from an initial distribution for $n = 2$, and, to determine the probabilities for electron capture, excitation, and ionization in collisions with $\text{H}(2s)$, we divide the phase space in nonoverlapping boxes, as explained in Ref. [40]. We obtain the probabilities for collisions with $\text{H}(2s)$ from the subset of trajectories that initially lie in the $l = 0$ box. The CTMC calculation provides total and partial cross sections for all processes simultaneously, but the standard microcanonical initial distribution has important limitations, in particular, for collisions with $\text{H}(1s)$, which have motivated us to perform calculations with both the microcanonical (m-CTMC) and the hydrogenic (h-CTMC) initial distributions.

In order to check the usefulness of the GTDSE method to calculate excitation cross sections, not considered in previous studies, we have calculated cross sections for excitation of

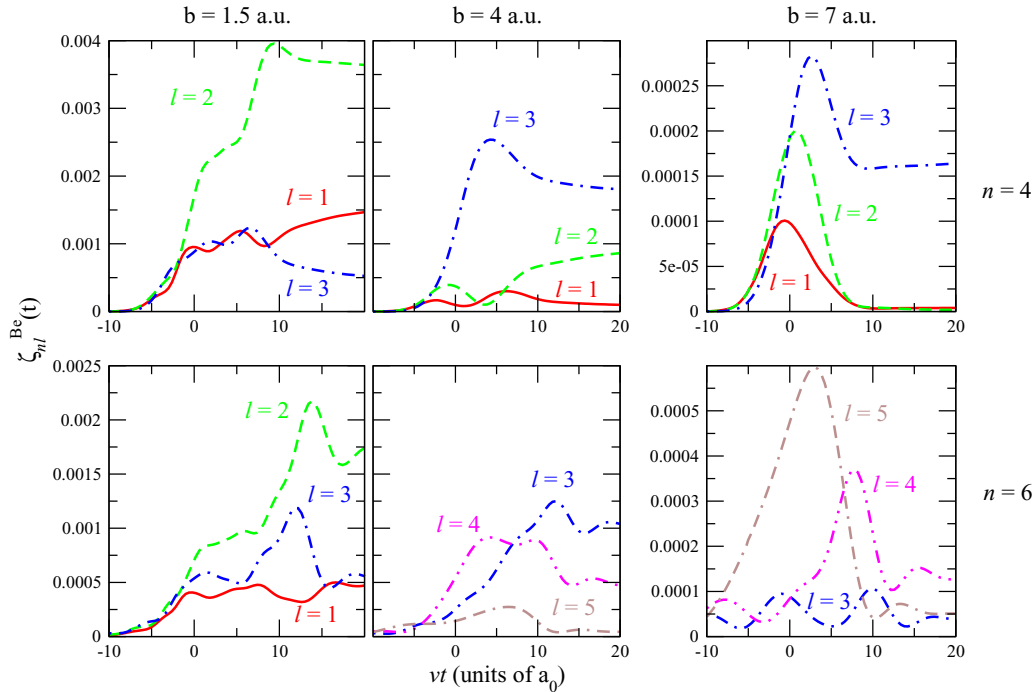


FIG. 11. Time evolution of $\zeta_{nl}^{\text{Be}}(t)$ [Eq. (18)] as functions of vt for $E = 100$ keV/u, and the values of b and n indicated in the figure.

$\text{H}(1s)$ [Eq. (21)]. Our results show a very good agreement with previous close-coupling results. The GTDSE has been then applied to check the CTMC excitation cross sections from $\text{H}(2s)$ at two energies ($E = 20$ and 100 keV/u). We find that the m-CTMC underestimates the n partial cross sections, while the h-CTMC shows a reasonable agreement for excita-

tion into $\text{H}(n = 4, 5)$, which supports the application of this method to calculate excitation cross sections into high n -lying excited levels, which are very difficult to accurately compute with close-coupling or lattice semiclassical treatments.

The analysis of the transition probabilities and the time evolution of the electron wave function in the GTDSE calculation provides some insight into the mechanism of the excitation process in ion collisions with $\text{H}(2s)$. This mechanism has two main ingredients: (1) the $2s - 2p$ Stark mixing and (2) the transitions from $2s$ and $2p$ to excited nl subshells, which take place following the $\Delta l = \pm 1$ selection rule. As the energy increases, the Stark mixing becomes less important and the population of states with $l \geq 2$ decreases. At relatively low velocities, the nl partial cross sections increase with l with a statistical behavior for $l < 4$, but the sequential mechanism requires more than two steps for the excitation to $l \geq 3$, which leads to a decrease of the corresponding cross sections.

The cross sections for EC from $\text{H}(2s)$, calculated with m-CTMC and h-CTMC, show good agreement, as previously found for collisions of multicharged ions with $\text{H}(n = 2)$. This result, together with the satisfactory agreement of CTMC and GTDSE results, supports the validity of the widely applied m-CTMC method for EC from excited targets. The nl partial EC cross sections exhibit a similar behavior to that for collisions of other ions with $\text{H}(n = 2)$ with a shift to lower l 's of the maximum of the l distribution, as the energy increases.

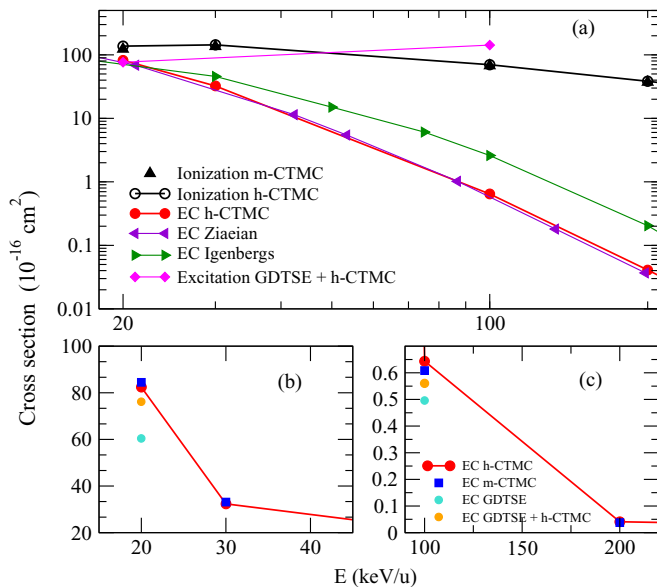


FIG. 12. (a) Total cross sections for excitation, electron capture, and ionization in $\text{Be}^{4+} + \text{H}(2s)$ collisions. The comparison of electron capture total cross sections calculated using GTDSE, h-CTMC, and m-CTMC methods at $E = 20$ and 100 keV/u is presented in panels (b) and (c), respectively.

ACKNOWLEDGMENT

This work has been partially supported by Ministerio de Economía and Competitividad (Spain), Project No. FIS2017-84684-R.

- [1] R. C. Isler, An overview of charge-exchange spectroscopy as a plasma diagnostic, *Plasma Phys. Controlled Fusion* **36**, 171 (1994).
- [2] R. M. McDermott, R. Dux, T. Pütterich, B. Geiger, A. Kappatou, A. Lebschy, C. Bruhn, M. Cavedon, A. Frank, N. den Harder, E. Viezzer, and the ASDEX Upgrade Team, Evaluation of impurity densities from charge exchange recombination spectroscopy measurements at ASDEX upgrade, *Plasma Phys. Controlled Fusion* **60**, 095007 (2018).
- [3] R. McDermott, R. Dux, F. Guzman, T. Pütterich, R. Fischer, A. Kappatou, and the ASDEX Upgrade team, Development of Ar¹⁶⁺ charge exchange recombination spectroscopy measurements at ASDEX upgrade, *Nucl. Fusion* **61**, 016019 (2021).
- [4] R. Hoekstra, H. Anderson, F. W. Blik, M. von Hellermann, C. F. Maggi, R. E. Olson, and H. P. Summers, Charge exchange from D(n= 2) atoms to low-z receiver ions, *Plasma Phys. Controlled Fusion* **40**, 1541 (1998).
- [5] K. Igenbergs, J. Schweinzer, and F. Aumayr, Charge exchange in Be⁴⁺-H(n= 1, 2) collisions studied systematically by atomic-orbital close-coupling calculations, *J. Phys. B* **42**, 235206 (2009).
- [6] E. Delabie *et al.*, Consistency of atomic data for the interpretation of beam emission spectra, *Plasma Phys. Controlled Fusion* **52**, 125008 (2010).
- [7] I. Ziaeiian and K. Tórkésy, State-selective charge exchange cross sections in Be⁴⁺ - H(2lm) collision based on the classical trajectory monte carlo method, *Eur. Phys. J. D* **75**, 138 (2021).
- [8] D. Delibašić, N. Milojević, I. Mančev, and D. Belkić, Electron transfer from atomic hydrogen to multiply-charged nuclei at intermediate and high energies, *At. Data Nucl. Data Tables* **139**, 101417 (2021).
- [9] N. W. Antonio, C. T. Plowman, I. B. Abdurakhmanov, I. Bray, and A. S. Kadyrov, Integrated total and state-selective cross sections for bare beryllium ion collisions with atomic hydrogen, *J. Phys. B* **54**, 175201 (2021).
- [10] R. Abrines and I. C. Percival, Classical theory of charge transfer and ionization of hydrogen atoms by protons, *Proc. Phys. Soc.* **88**, 861 (1966).
- [11] D. J. W. Hardie and R. E. Olson, Charge transfer and ionisation processes involving multiply charged ions in collision with atomic hydrogen, *J. Phys. B* **16**, 1983 (1983).
- [12] J. S. Cohen, Classical phase-space distributions for atomic hydrogen collisions, *J. Phys. B* **18**, 1759 (1985).
- [13] M. J. Rakovic, D. R. Schultz, P. C. Stancil, and R. K. Janev, On quantum-classical correspondence in classical studies of atomic processes, *J. Phys. A* **34**, 4753 (2001).
- [14] C. Illescas and A. Riera, Classical study of single-electron capture and ionization processes in A^{q+} + (H, H₂) collisions, *Phys. Rev. A* **60**, 4546 (1999).
- [15] L. F. Errea, C. Illescas, L. Méndez, B. Pons, A. Riera, and J. Suárez, Classical and semi-classical treatments of Li³⁺, Ne¹⁰⁺ + H(1s) collisions, *J. Phys. B* **37**, 4323 (2004).
- [16] L. F. Errea, C. Illescas, L. Méndez, B. Pons, A. Riera, and J. Suárez, Charge transfer and ionization involving argon ions and neutral hydrogen, *J. Phys. B* **39**, L91 (2006).
- [17] L. F. Errea, F. Guzmán, C. Illescas, L. Méndez, B. Pons, A. Riera, and J. Suárez, Recommended data for capture cross sections in B⁵⁺ + H collisions, *Plasma Phys. Controlled Fusion* **48**, 1585 (2006).
- [18] A. Jorge, L. Errea, C. Illescas, and L. Méndez, Calculation of ionization and total and partial charge exchange cross sections for collisions of C⁶⁺ and N⁷⁺ with H, *Eur. Phys. J. D* **68**, 227 (2014).
- [19] F. Guzmán, L. F. Errea, C. Illescas, L. Méndez, and B. Pons, Calculation of total cross sections and effective emission coefficients for B⁵⁺ collisions with ground-state and excited hydrogen, *J. Phys. B* **43**, 144007 (2010).
- [20] R. K. Janev and L. P. Presnyakov, Single-electron excitation and ionisation processes in atom-multicharged-ion collisions, *J. Phys. B* **13**, 4233 (1980).
- [21] W. Fritsch and K.-H. Scharfner, Scaling properties of target excitation cross sections in collisions between atoms and multiply charged ions, *Phys. Lett. A* **126**, 17 (1987).
- [22] V. Rodríguez and J. Miraglia, Scaling properties in hydrogen excitation by multiply charged ions at intermediate energies, *Phys. Lett. A* **138**, 123 (1989).
- [23] C. O. Reinhold, R. E. Olson, and W. Fritsch, Excitation of atomic hydrogen by fully stripped ions, *Phys. Rev. A* **41**, 4837 (1990).
- [24] J. Suarez, F. Guzman, B. Pons, and L. F. Errea, Excitation cross sections for Li³⁺, Ne¹⁰⁺ and Ar¹⁸⁺ + H(1s) collisions of interest in fusion plasma diagnostics, *J. Phys. B* **46**, 095701 (2013).
- [25] L. F. Errea, L. Méndez, B. Pons, A. Riera, I. Sevilla, and J. Suárez, Semiclassical treatment of excitation and electron loss in A^{q+} + H(1s) collisions using spherical bessel functions, *Phys. Rev. A* **74**, 012722 (2006).
- [26] D. R. Schultz, M. R. Strayer, and J. C. Wells, Lattice, Time-Dependent Schrödinger Equation Solution for Ion-Atom Collisions, *Phys. Rev. Lett.* **82**, 3976 (1999).
- [27] M. Chassid and M. Horbatsch, Electron emission characteristics in p - H(1s) collisions from numerical solutions of the time-dependent Schrödinger equation, *Phys. Rev. A* **66**, 012714 (2002).
- [28] T. Minami, M. S. Pindzola, T.-G. Lee, and D. R. Schultz, Lattice, time-dependent Schrödinger equation approach for charge transfer in collisions of Be⁴⁺ with atomic hydrogen, *J. Phys. B* **39**, 2877 (2006).
- [29] A. Jorge, J. Suárez, C. Illescas, L. F. Errea, and L. Méndez, Application of a grid numerical method to calculate state-selective cross sections for electron capture in Be⁴⁺ + H(1s) collisions, *Phys. Rev. A* **94**, 032707 (2016).
- [30] C. Illescas, M. A. Lombana, L. Méndez, I. Rabadán, and J. Suárez, A classical and semiclassical study of collisions between X^{q+} ions and water molecules, *Phys. Chem. Chem. Phys.* **22**, 19573 (2020).
- [31] J. Suarez, S. Farantos, S. Stamatidis, and L. Lathouwers, A method for solving the molecular schrödinger equation in cartesian coordinates via angular momentum projection operators, *Comput. Phys. Commun.* **180**, 2025 (2009).
- [32] L. Errea, C. Illescas, L. Méndez, I. Rabadán, and J. Suárez, Lattice description of electron loss in high-energy H⁺ + H₂O collisions, *Chem. Phys.* **462**, 17 (2015).
- [33] R. Guantes and S. C. Farantos, High order finite difference algorithms for solving the schrödinger equation in molecular dynamics, *J. Chem. Phys.* **111**, 10827 (1999).
- [34] C. Leforestier, R. Bisseling, C. Cerjan, M. Feit, R. Friesner, A. Guldberg, A. Hammerich, G. Jolicard, W. Karrlein, H.-D. Meyer, N. Lipkin, O. Roncero, and R. Kosloff,

- A comparison of different propagation schemes for the time dependent Schrödinger equation, *J. Comput. Phys.* **94**, 59 (1991).
- [35] D. Dundas, J. F. McCann, J. S. Parker, and K. T. Taylor, Ionization dynamics of laser-driven H_2^+ , *J. Phys. B* **33**, 3261 (2000).
- [36] R. Kosloff and D. Kosloff, Absorbing boundaries for wave propagation problems, *J. Comput. Phys.* **63**, 363 (1986).
- [37] U. D. Giovannini, A. H. Larsen, and A. Rubio, Absorbing boundaries for wave propagation problems, *Eur. Phys. J. B.* **88**, 56 (2015).
- [38] C. Illescas, I. Rabadán, and A. Riera, Illustration of the role of saddle-point and molecular-type ionization mechanisms in atomic collisions, *Phys. Rev. A* **57**, 1809 (1998).
- [39] R. E. Olson, n, l distributions in $A^{q+} + H$ electron-capture collisions, *Phys. Rev. A* **24**, 1726 (1981).
- [40] R. L. Becker and A. D. MacKellar, Theoretical initial l dependence of ion-Rydberg-atom collision cross sections, *J. Phys. B* **17**, 3923 (1984).
- [41] L. F. Errea, C. Illescas, L. Méndez, B. Pons, A. Riera, and J. Suárez, Accuracy of the classical trajectory monte carlo method for electron capture in Li^{3+} and $Ne^{10+} + H(1s)$ collisions, *Phys. Rev. A* **70**, 052713 (2004).
- [42] V. D. Rodriguez and J. E. Miraglia, Hydrogen excitation by antiproton and multicharged-ion impact, *J. Phys. B* **25**, 2037 (1992).
- [43] I. Ziaean and K. Tökési, Interaction of Be^{4+} and ground state hydrogen atom-Classical treatment of the collision, *Atoms* **8**, 27 (2020).
- [44] L. F. Errea, J. D. Gorfinkiel, C. Harel, H. Jouin, A. Macías, L. Méndez, B. Pons, and A. Riera, Total and partial cross-sections of electron transfer processes with hydrogen gas targets: Be^{4+} , $B^{5+} + H(1s)$, $H(2s)$, *Phys. Scr.* **T62**, 27 (1996).
- [45] Z. Chen, B. D. Esry, C. D. Lin, and R. D. Piacentini, Excitation and ionization of $h(2s)$ by proton impact, *J. Phys. B* **27**, 2511 (1994).
- [46] K. Igenbergs, Calculation of cross sections relevant for diagnostics of hot fusion plasmas, Ph.D. thesis, Technische Universität Wien, 2011.